ORIGINAL RESEARCH

# Evaluating the Effect of Fiber Addition on Seismic Performance of Segmental Tunnel Lining

Saeed Farokhi Zadeh [1], Majid Moradi[2], Ata Hojatkashani [3*]

## Abstract

Since the analysis of underground structures in seismic conditions was more based on non-linear terrestrial environment and linear structure, regarding nonlinear behavior of soil and tunnel against earthquake was of paramount significance in order to achieve real responses in practice. The use of polypropylene fibers in concrete materials can help improve the performance of concrete members. In this regard, after verifying the behavioral model of fiber-reinforced concrete seen in the structure of the tunnel and using an article by Conforti et al., the nonlinear seismic analysis of the ground and the structure of the water transmission tunnel of Amirkabir Dam to Tehran refinery no. 6 was performed by a time-history method and through ABAQUS software and concrete damage plasticity model for concrete lining and mohr-coloumb model for host soil of tunnel. Simulations were performed for the fibers with percentages of 0, 0.7, 1 and 1.5. Then, compressive and tensile stresses, compressive and tensile strains, and compressive and tensile failures were obtained while tunnel lining in the mentioned conditions. Since then, normal and shear stresses and normal and shear displacements of the longitudinal joints of the tunnel were examined. Finally, this paper studied the analytical relationships that existed in the ACI 544.7R-16 regulations and the moment-force diagram for the different percentages of fibers for the joint with the maximum normal stress under earthquake records were compared. The results revealed that the tunnel lining and its longitudinal joints using polypropylene fibers with a volume percent of 1.5 had a better performance than other percentages against earthquakes.

**Key words:** Water Transmission Tunnel, Earthquake Loads, Fibers, Tunnel Lining, Concrete Damage Model, Nonlinear Analysis

## 1. Introduction

In designing and analyzing the underground structures such as tunnels, it was assumed that the main criterion was the deformation of the structure and the surrounding environment since their seismic response to imposed deformation was very sensitive. Before 995, the design of tunnels was not taken place due to withstanding dynamic loads, but their design process reformed at the same time with the occurrence of earthquakes of the 1990s and serious failures created in some of the tunnels [1]. These earthquakes were such as Kobe-Japan earthquake (1995), in which the Daikai subway station collapsed, Chi-Chi earthquake (1999) in central Taiwan on September 21, in which many tunnels were seriously ruined and also Dozeke earthquake (1999) in Turkey on November 12, in which Bolu Twin Tunnel was extensively destroyed [2].

In the studies by Mayoral et. Al. (2016) appraised the vulnerability and the degree of damages to various tunnel under the earthquake [3]. Hashash in the years of 2001 and 2004 stressed this important point that the tunnel structure should be investigated in terms of ductility and resistance to earthquakes. Also, it was recommended that in order to provide sufficient ductility in the tunnel lining while an earthquake, the force

*Corresponding author, ata_hojat@aut.ac.ir

1,3. Department of civil Engineering, South Tehran Branch, Islamic Azad University, Tehran, Iran
2. Earthquake Engineering, faculty of Civil Engineering, University of Noshirvani, Babol, Iran.

reduction factor should be equal to the provided ductility for the tunnel [4].

Concrete is known by a very high and considerable compressive strength, but it acts in weak tensile strength. It can almost be noted that the tensile strength of concrete is about 11% of its compressive strength [5]. Hence, the primary utilization of concrete was only observed in cases where the concrete was pressurized, such as load-bearing walls or domes [6]. In order to overcome the weakness of concrete in traction, concrete must be integrated with a material that was resistant to traction. So, in the early 11th century, steel bars were used for reinforcement of concrete [7]. The arrangement of steel in concrete can be seen in one shape or different shapes in order to increase the tensile strength of concrete. Therefore, steel bars can be provided in the shapes of square, rectangular, circular, or a combination of them. Making use of fiber in concrete, which was to improve its mechanical properties, was first introduced by Romualdi and Batson in 1990 [8].

Fibers could be separated into different categories. One of these categories was attributed to the material from which the fibers were made. Fibers could be natural (like animal hair), mineral or synthetic. The other fibers category was recognized based on their properties [9]. For example, their resistance to fire, stiffness, or tensile strength. In the early 1311s, they were more inclined towards the production of fiber-reinforced concrete with high ductility. In the case of using FRC, the durability of concrete increased, and no significant change was observed in the ductility of concrete [10]. Fibers could be portioned based on different parameters:

1. Based on the type of material of their constituents: natural fibers (such as horsehair, hemp, or coconut fiber), mineral fibers (asbestos, glass or carbon), and synthetic fibers (such as polypropylene) [11].

2- Based on their physical or chemical properties: density, surface roughness, chemical resistance, the reaction of fibers with cement and resistance to fire or flammability, and so on.

3. Mechanical properties of fibers. Such as tensile strength, elastic modulus, stiffness, ductility, fiber length change until rupture, surface adhesion, and so on.

4. Geometric properties of fibers: length, diameter or radius of fibers, the shape of the cross-section of fibers and its longitudinal profile [12-14].

Synthetic fibers of polypropylene were applied in the current study.

As mentioned in previous researches, the use of fibers in concrete can help improve various properties. Therefore, in this research, it has been tried to investigate the effect of using polypropylene fiber concrete in improving the seismic performance of existing tunnels in Amirkabir Dam. Also, in this research, it has been tried to examine the analytical relationships in ACI 544.7R-16 and discuss the effect of using the mentioned fibers in these relationships.

## 2. Types and the application of Fiber-Reinforced Concrete

It was recommended to divide fiber-reinforced concretes into tensile stiffness and tensile softness based on their tensile response [15]. The most important difference lay between concrete and tensile softening behavior, and tensile stiffening behavior was that in concrete with tensile softening behavior, a crack was formed and grew [16]. But, several parallel micro-cracks were formed in the tensile stiffening behavior. This was the difference in behavior that finally appeared significant structural differences in the durability and load-carrying capacity of the structure [17].

Another method portioning the fiber-reinforced concretes was the determination of them based on the amount of fiber inside them. The volume ratio of fibers was equal to the volume of fibers used in concrete to the total volume of the compound. Regarding the difference in the specific weight of the fibers, it was obvious that two different types of fibers with the same

volume ratio were not necessarily with the same mass ratio [18]. The fibers were prepared and purchased according to their weight, but the mechanical features of the compound were evaluated on the basis of the volume ratio of the fibers. Typically, 1% volume of steel fibers in a conventional concrete included about 11 kg/$m^3$ of fibers, while concrete with 1% volume of polypropylene fibers encompassed only about 3.2 kg / $m^3$ of fibers [19].

Making use of fibers led to a reduction in the required thickness of the slabs, an increase in the permissible distance between the supports and in the ductility in the first days of concreting, and also a reduction in the initial cracks [20]. Moreover, fibers were much more economical than steel meshes because of high specific surface area, reduced workshop costs, reduced individual error potential at the workplace and optimizing, and saving time. Fiber-reinforced concrete was observed as the best alternative to steel bars in the use of thin membrane structures. It alone was more practical for thin structures and when resistance and strength were significant but not decisive, such as prefabricated parts, tunnel lining, and shotcrete [21]. Particularly, HPFRC concretes were seen on bridge decks and coastal and hydraulic specific structures, reservoirs, and shelters [22].

## 3. Designing Joints between Segments in Tunnels

In tunnel analysis methods, there was an assumption that the tunnel lining section was continuous. When the tunnel was dug with tunnel boring machines (TBM), the tunnel lining was usually mounted in the form of a segment. These segments were linked to each other by means of bolts. The joints between the segments should be designed in such a way to compromise the forecasted deformation of the ground. The designer probably observed the joint between the two segments as elastic, or if the non-elastic behavior was predicted in more detail, the interaction between the ground and the lining should be taken into consideration [23].

Conforti et al. (2017) conducted experimental research and studied the effect of fibers on concrete. The results of this laboratory research were adopted in order to verify the used behavioral model. This paper was conducted to verify and was located in the Monte Liro area of Panama country, which was bored through the TBM method. The characteristics of this tunnel were as follows [24]:

**Table1. Characteristics of studied tunnel segments for verification [24]**

| Value | Parameter |
|---|---|
| 7.88 | Total length of the tunnel (km) |
| 3200 | Segment internal diameter (mm) |
| 250 | Segment thickness (mm) |
| 3700 | Segment outer diameter (mm) |
| 1200 | Segment depth (mm) |
| 4 | Number of main segments in each ring |
| 2 | Number of key segments in each ring |

Table 2 represented the properties of the polypropylene fibers used in the study.

**Table2. Properties of fibers used in Monte Liro tunnel [24]**

| **Value** | **Property** |
|---|---|
| 54 mm | Length |
| 0.81mm | Diameter |
| 67 | Dimensions ratio |
| 552 MPa | Minimum tensile strength |
| 6000 MPa | Modulus of elasticity |
| 910 kg/$m^3$ | density |

Yield and final strength for bar 10 were regarded based on Eurocode2 standard 475 MPa and 572 MPa, respectively [24].

## 4. Non-Linear Quasi-Static Modeling of Monte Liro Tunnel Segment

In order to model the Monte Liro tunnel segment, ABAQUS and damage software was applied for the concrete lining of the tunnel. Concrete damage plasticity model was used with the purpose of describing non-linear materials in fiber-reinforced concrete lining of the tunnel in ABAQUS software. This behavioral model was the most complex and popular model for concrete modeling in this software. In this model, the nonlinear behavior of concrete was simulated through the concepts of damage isotropic elastic and tensile and compressive plastics. The relations 1-4 were presented for compressive behavior of fiber-free concrete with respect to Eurocode2 standard [25]:

Where, $f_{cm}$ indicated the cylindrical compressive strength, which was equal to 48.2 MPa. $\sigma_c$ was compressive strength, $\varepsilon_c$ was a compressive strain, $\varepsilon_{c_1}$ was compressive strain at maximum compressive strength, and $E_{cm}$ was the modulus of elasticity.

Figure 1 revealed the diagram of the compressive stress-strain of fiber-free concrete.

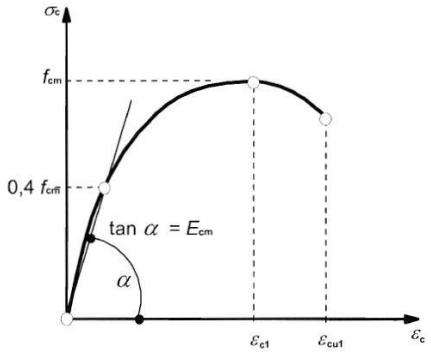


**Figure 1. Compressive stress-strain of fiber-free concrete.**

$$\frac{\sigma_c}{f_{cm}} = \frac{k\eta - \eta^2}{1 + (k-2)\eta} \quad (1)$$

$$\eta = {\varepsilon_c}/{\varepsilon_{c_1}} \quad (2)$$

$$k = 1.05E_{cm} \times \left|\varepsilon_{c_1}\right|/f_{cm} \quad (3)$$

$$E_{cm} = 22[(f_{cm})/10]^{0.3} \quad (4)$$

$$\boldsymbol{d_c = \frac{1}{e^{-1/m_c^{hf}} - 1}\left(e^{-\varepsilon_{c,norm}^{in}/m_c^{hf}} - 1\right)}$$

Hsu relations were applied for the concrete tensile behavior model [26]. The tensile stress-strain relation was exhibited in the following relations.

$$f_t = f_{ct}\left(\frac{\varepsilon_{ct}}{\varepsilon_t}\right) \quad (5)$$

$$f_{ct} = 0.63 \times \sqrt{f_{cm}} \quad (6)$$

Where, $f_{ct}$ and $\varepsilon_{ct}$ were attributed to the tensile strength and the tensile strain, respectively.

Table 3 represented the plastic parameters of fiber-free concrete and their values.

**Table3. Plastic parameters of fiber-free concrete**

| Value | Parameter |
|---|---|
| 30 | Dilation angle of concrete |
| 0.1 | the eccentricity of concrete (ϵ) |
| 1.16 | The ratio of the yield stress of biaxial compression to uniaxial compression |
| 0.667 | The ratio of secondary stress to the maximum amount of tension |
| 0.001 | The viscosity parameter of concrete equilibrium equations |

The stress-strain curve extracted from the fibcode2010 regulation was adopted for the compressive behavior of fiber-reinforced concrete [27]. The extracted diagram from the Yuan article was used for the tensile behavior of fiber-reinforced concrete [28]. Huang relations were applied for the plastic range and fiber-reinforced concrete failure [29].

**Table4. Huang Relations**

| **Eq.** | **Eq. No** |
|---|---|
| $\boldsymbol{\varepsilon_c^{pl} = \varepsilon_c^{in} - \frac{d_c}{(1-d_c)}\frac{\sigma_c}{E_{cm}}}$ | (7) |
| $\boldsymbol{\varepsilon_t^{pl} = \varepsilon_t^{ck} - \frac{d_t}{(1-d_t)}\frac{\sigma_t}{E_{cm}}}$ | (8) |

(9)

$$d_t = \frac{1}{e^{-1/m_t^{hf}} - 1}\left(e^{-\varepsilon_{t,norm}^{ck}/m_t^{hf}} - 1\right) \quad (10)$$

$$m_c^{hf} = m_c\left(1 + a_{m1}\lambda_{sf} + b_{m1}\lambda_{pf}\right) \quad (11)$$

$$m_t^{hf} = m_t\left(1 + a_{m2}\lambda_{sf} + b_{m2}\lambda_{pf}\right) \quad (12)$$

$$\lambda_{sf} = V_{sf}\left(l_{sf}/d_{sf}\right) \quad (13)$$

$$\lambda_{pf} = V_{pf}\left(l_{pf}/d_{pf}\right) \quad (14)$$

$$\varepsilon_{c,norm}^{in} = \varepsilon_c^{in}/\varepsilon_{cu}^{in} \quad (15)$$

$$\varepsilon_{t,norm}^{ck} = \varepsilon_t^{ck}/\varepsilon_{tu}^{ck} \quad (16)$$

| Patameter | Value |
|---|---|
| $\varepsilon_{cu}^{in}$ , $\varepsilon_{tu}^{ck}$ | 0.033 , 0.0033 |
| $m_c$ , $m_t$ | 0.1 , 0.05 |
| $a_{m1}$ , $b_{m1}$ , $a_{m2}$ | 0.452, 0.054, 0.628 |
| $b_{m2}$ | 0.156 |

**Definition**

$\varepsilon_{c,norm}^{in}$: Normal compressive strain
$\varepsilon_{cu}^{in}$: Final compressive strain
$\varepsilon_{t,norm}^{ck}$: Normal tensile strain
$\varepsilon_{tu}^{ck}$: Final tensile strain
$m_c$ و $m_t$ : Parameters responsible for controlling the rate of damage development.
$m_c^{hf}, m_t^{hf}$ : Parameters responsible for controlling the damage rate for fiber-reinforcement concrete.
$a_{m1}, b_{m1}, a_{m2}, b_{m2}$: Constant parameters achieved from laboratory researches
$\lambda_{sf}$: A parameter dependent on volume percent, length, and diameter of steel fibers.
$\lambda_{pf}$ : A parameter dependent on the volume percent, length, and diameter of polypropylene fibers.
$V_{pf}$ : Volume percent of polypropylene fibers, which was equal to 1.1% in this study.

The plastic parameters of fiber-reinforced concrete were as below:

A) $K_c^{hf}$ Parameter (the ratio of secondary stress to maximum tensile value):

$$K_c^{hf} = K_c.\frac{k_t}{k_c} \quad (17)$$

$$k_t = 1 + 0.08\lambda_{sf} + 0.132\lambda_{pf} \quad (18)$$

$$k_c = 1 + 0.056\lambda_{sf} \quad (19)$$

B) $\sigma_{b0}^{hf}/\sigma_{c0}^{hf}$ Parameter (the ratio of yield stress of biaxial compression to uniaxial compression)

$$\frac{\sigma_{b0}^{hf}}{\sigma_{c0}^{hf}} = \frac{k_t^2}{0.132k_c}\left[\left(0.728 - \frac{0.749}{k_t}\right) + \sqrt{\left(0.728 - \frac{0.749}{k_t}\right)^2 + \frac{0.03}{k_t^2}}\right] \quad (20)$$

C) $\psi^{hf}$ Parameter (Dilation angle of concrete)

$$\psi^{hf} = \psi_0\left(1 - a_\psi\lambda_{sf} - b_\psi\lambda_{pf}\right) \quad (21)$$

$\psi_0$: Dilation angle for normal concrete
$a_\psi$ : Constant parameters achieved from laboratory researches which were equal to 0.861.
$b_\psi$ : Constant parameters achieved from laboratory researches which were equal to 0.097.

## 5.Verification

Figure 2 exhibited the load-displacement diagram of a sample containing fibers-free concrete and fiber-reinforced concrete extracted from the article [24]. The horizontal axis indicated the displacement in the center of the segment mouth in millimeters, and the vertical axis represented the amount of load in kN.

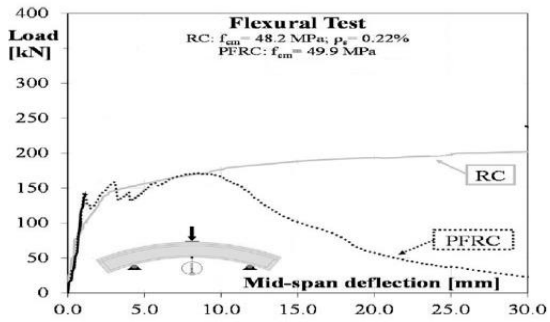


Figure 2. Load-displacement diagram of a sample containing fibers-free concrete and fiber-reinforced concrete

Figure 3 revealed the load-displacement diagram derived from the ABAQUS software for the fiber-free concrete sample.

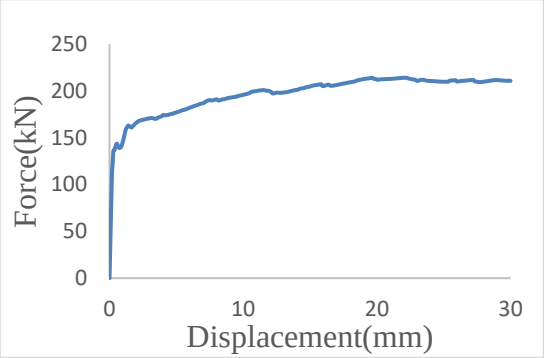


**Figure 3. Load-displacement diagram derived from the ABAQUS software for the fiber-free concrete sample.**

The load-displacement diagram obtained from the software for the fiber-reinforcement concrete sample was observed in figure 4.

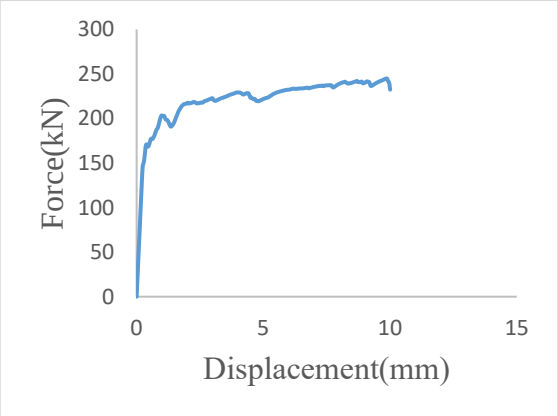


**Figure 4. Load-displacement diagram obtained from the FE software for the fiber-reinforcement concrete.**

Figure 5 was related to a comparison of the load-displacement diagram extracted from the paper and the software for the sample containing fiber-reinforced concrete. The blue curve represented the output of the software, and the gray diagram was attributed to the results of the paper, which were observed with the same behaviors.

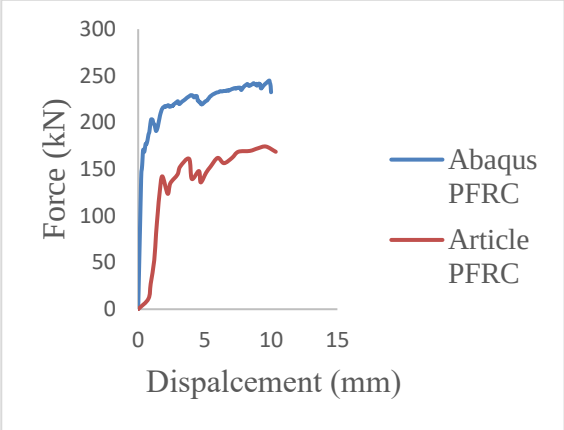


**Figure 5. Comparison of the load-displacement diagram extracted from the referenced article and FE software for the sample containing fiber-reinforced concrete**

## 6. Studied Tunnel

The selected tunnel for this study was the water transmission tunnel of Amirkabir Dam to Tehran refinery no. 6. This tunnel passed through different rock masses, which most of them were made of igneous rocks. The desired section was selected at 2600 km. The height of overburden in this section was 40 m. The physical characteristics and rock mechanics of this section were showed in table 5.

**Table 5. Strength properties of rock mass for the desired section based on design consultant studies**

| Friction angle | Adhesion | Poisson's ratio | Modulus of deformability | Special weight | characteristics |
|---|---|---|---|---|---|
| Degree | MPa | - | GPa | $Kg/m^3$ | **Unit** |
| 49.6 | 1.35 | 0.25 | 6 | 2700 | **Value** |

The bored section of this tunnel was in the shape of a circle. The radius of this tunnel was equal to 1.95m. Segmental lining, along with six-segment pieces (5+1) was used as a maintenance system. The properties of the segmental lining were presented in tables 6, 7, and 8. The parameters of the prefabricated concrete parts were derived from the design consultant studies, and the contact surface

parameters between the segment and the surrounding environment and between the two segments were mainly came from resources [30].

**Table6. Properties of prefabricated concrete parts (segments) for the desired section based on the design consultant studies [30]**

| Specification | Unit | Value |
|---|---|---|
| Special weight | $Kg/m^3$ | 2500 |
| Modulus of deformability | GPa | 30.2 |
| Poisson's ratio | - | 0.2 |
| Adhesion | MPa | 5.5 |
| Friction angle | Degree | 55 |
| Uniaxial compressive strength | MPa | 40 |
| Uniaxial tensile strength | MPa | 3.2 |

**Table 7. Properties of the contact surface between the two segments for the desired section based on the design consultant studies [30]**

| Specification | Unit | Value |
|---|---|---|
| Adhesion | MPa | 0.75 |
| Friction angle | Degree | 45 |
| Shear stiffness | $Gpa/m$ | 12.58 |
| Normal stiffness | $Gpa/m$ | 16.7 |

**Table 8. Properties of contact surface between segment and surrounding environment for the desired section based on the design consultant studies [30]**

| Specification | Unit | Value |
|---|---|---|
| Adhesion | MPa | 0.6 |
| Friction angle | Degree | 35 |
| Shear stiffness | $Gpa/m$ | 2.4 |
| Normal stiffness | $Gpa/m$ | 4 |

## 7. Reviewing the Results of the analysis of the tunnel rings containing longitudinal joints

### *A) Reviewing Stress Changes*

This part investigated the main stress, which was the representative of compressive and tensile stresses for 0, 0.7, 1, and 1.5 percentages of polypropylene fibers under seven earthquake records as displayed in blue, red, gray, and yellow, respectively. Crushing was known as the major (85%) part of the compressive stress adapted to the software. In this paper, compressive stress on the software was considered to be 40 MPa, and the crushing stress 34 MPa. These given compressive stresses were reviewed based on the conducted test at Amirkabir University. It was understood that tensile stress was equal to 0.1-0.07 compressive strength, which here was equal to 3.2 MPa.

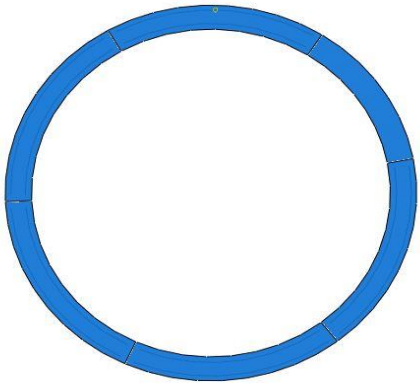

**Figure 6. Position of longitudinal joints of the tunnel ring**

Figure 7 shows the comparison of compressive stresses of the tunnel-ring in the percentage of different fibers under the seven earthquake records. Generally, adding fiber with any percentage to concrete under the seven earthquake record resulted in the reduction of the compressive stress of the tunnel-ring, which was due to state that some parts of the concrete cracked in 0% of the fibers and unloading share of the parts increased. By adding fibers, the parts that

were cracked in 0% fibers would no longer crack, and other parts of the concrete would participate in unloading, and their share of the unloading would be lessened, leading to the less compressive stress of ring. The maximum compressive stress for concrete with 0% fiber was observed in the Kocaeli earthquake. The maximum compressive stress was attributed to concrete with 1.5% fibers under Kocaeli earthquake and was equal to 38.47 MPa, declaring that the concrete, in this case, was involved in compressive crushing.

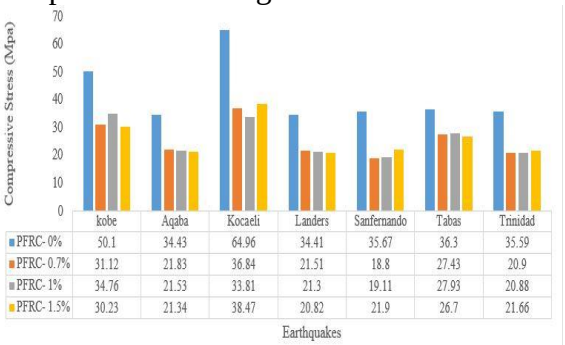


**Figure 7. Comparison of compressive stresses at longitudinal joints of the tunnel-ring under seven earthquake records**

A comparison of the tensile stresses of the tunnel-ring at different percentages of fibers under 7 earthquake records has been done. In 5 out of 7 earthquake records, tensile stress minimized by adding fibers to concrete, the reason for which was as same as the reason mentioned for previous compressive stress. But after adding fibers to concrete, tensile stress increased in the Aqaba and Kocaeli earthquakes. The maximum tensile stress was related to concrete with 1.5% fiber under the Kocaeli earthquake, and its value was equal to 2.61 MPa. Since this value was less than 3.2 MPa, it was represented that the concrete was not involved in tensile cracking.

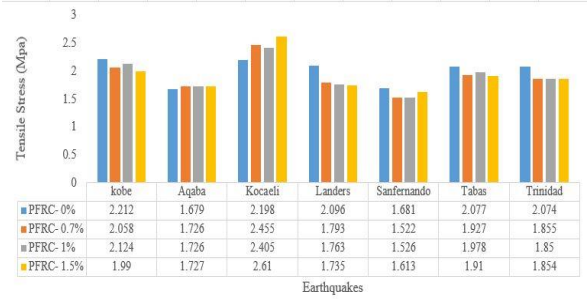


**Figure 8. A comparison of the tensile stresses of the tunnel-ring at different percentages of fibers**

***B) Reviewing the Failure***

Figure 9 displayed a comparison of the compressive failure of a tunnel-ring under seven earthquake records. In 6 of the 7 earthquakes imposed on the structure, the addition of fibers reduced the compressive failure. The maximum compressive failure in concrete with 0% fiber was under the Kocaeli earthquake, and its value was equal to 0.0001863. This value was less than the 0.97 failure given to the software, and the concrete was not involved in compressive crushing. The minimum compressive failure was related to concrete with 0.7% fiber under Sanfernando earthquake and was equal to 0.00000001504. This slight value of compressive failure declared the suitable impact of adding fibers to the intended structure.

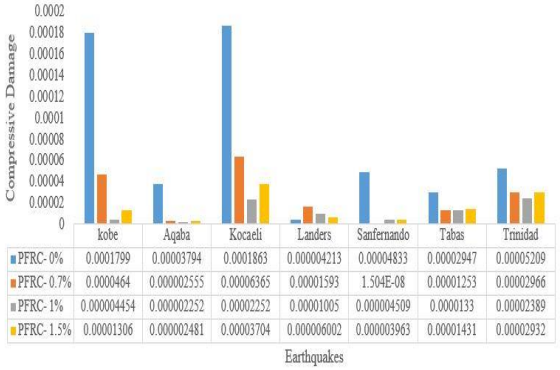


**Figure 9. Comparison of tunnel-ring compressive failure in different percentages of the fiber under 7 earthquake records**

Figure 10 respected a comparison of tunnel-ring tensile failure in different percentages of fibers under 7 earthquake records. The addition of fibers in all earthquakes showed a downward trend in tensile failure. The maximum tensile failure occurred in concrete with 0% fiber under the Kocaeli earthquake, the value of which was 0.9663 and was a bit less than the value of 0.96632 given to software. This represented that the concrete in this case was exposed to tensile cracking. The minimum tensile failure was seen in concrete with 0.7% fiber under Sanfernando earthquake, which was equal to

0.2123. This reduced value of tensile failure exhibited the suitable impact of adding fibers to the structure.

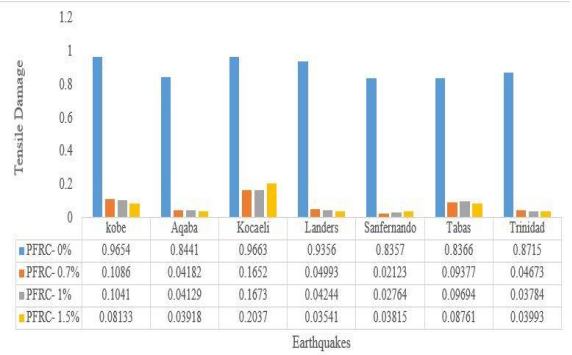


| | kobe | Aqaba | Kocaeli | Landers | Sanfernando | Tabas | Trinidad |
|---|---|---|---|---|---|---|---|
| PFRC- 0% | 0.9654 | 0.8441 | 0.9663 | 0.9356 | 0.8357 | 0.8366 | 0.8715 |
| PFRC- 0.7% | 0.1086 | 0.04182 | 0.1652 | 0.04993 | 0.02123 | 0.09377 | 0.04673 |
| PFRC- 1% | 0.1041 | 0.04129 | 0.1673 | 0.04244 | 0.02764 | 0.09694 | 0.03784 |
| PFRC- 1.5% | 0.08133 | 0.03918 | 0.2037 | 0.03541 | 0.03815 | 0.08761 | 0.03993 |

**Figure 10. Comparison of tunnel-ring Tensile failure in different percentages of the fiber under 7 earthquake records**

## 8. Examining the Results of Tunnel-Ring with Longitudinal joints

As previously mentioned, 6 prefabricated concrete pieces (5+1) were considered, and their arrangement position was represented in figure 17. The longitudinal joints were numbered from 1 to 6, respectively, and the sequences would be the same until the end. The joint 1 was the first joint at the top right. 6 contacts were considered at the contact surface between the two segments as well as 1 contact at the contact surface between the segments and the rock (peripheral joint). This part examined the effect of adding 0.7%, 1%, and 1.5% fibers on the results of the time-history analysis, which was consisted of shear stress, normal stress, shear displacement, and normal displacement, for longitudinal joints of a tunnel-ring.

### *A) Investigating Changes in Normal Stresses of Longitudinal Joints*

The conducted studies stated that the normal stress of the joints in 5 of the 7 earthquakes in most joints (at least 4 joints out of 6 joints) was in the maximum state of 1.5% fibers, showing the very suitable effect of fibers with volume percent of 1.5 on normal stress of tunnel-ring longitudinal joints. The maximum normal stress of the tunnel-ring joints in joint 3 occurred in the case of 1.5% fibers under 6 of the 7 studied earthquakes, indicating the sensitivity of the joint 3 for normal stress.

Figure 11 was attributed to a comparison of the maximum normal stress of joint 4 under the Kobe earthquake and joint 3 under the other earthquakes in the case of 1.5% fiber. It was deduced from this diagram that the maximum stress of the tunnel-ring joints under the Kocaeli earthquake was more considerable than that of other earthquakes.

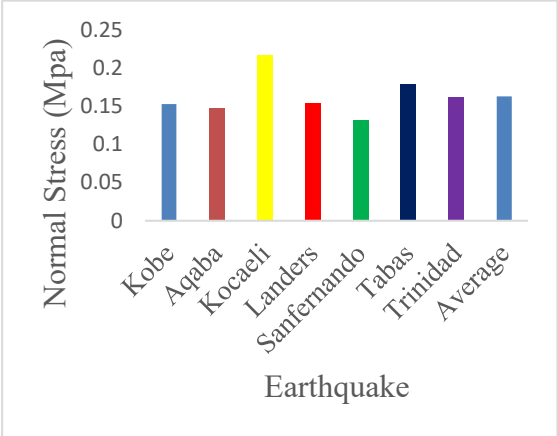


**Figure 11. Comparison of the maximum normal stress of joint 4 under the Kobe earthquake and joint 3 under the other earthquakes in the case of 1.5% fiber**

### *B) Investigating the Changes in Shear Stresses of Longitudinal joints*

The conducted studies showed that the shear stress of the joints in 5 of the 7 earthquakes in most joints (at least critical ast 4 joints out of 6 joints) was in the maximum state of 1.5% fibers, indicating the very suitable effect of fibers with volume percent of 1.5 on shear stress of tunnel-ring longitudinal joints. The maximum shear stress of the tunnel-ring joints at joint 4 was in the case of 0% fiber under 2 earthquakes, in the case of 1.5% fiber under 3 earthquakes, and totally it was maximized for 5 earthquakes. Moreover, this parameter was in the maximum state in joint 3 in the case of 0.7% fibers under 1 earthquake, in the case of 1.5% fibers under 1 earthquake and totally under 2 earthquakes. These values represented the sensitivity of the joints 4 relative to the other joints for shear stress.

Figure 12 was attributed to the comparison of maximum shear stress of joint 4 under Sanfernando and Tabas earthquakes in 0%

fiber and under Kobe, Aqaba and Trinidad earthquakes in 1.5% fiber and maximum shear stress of joint 3 under the Kocaeli earthquake in 1.5% fibers and under Landers earthquake in 0.7% fibers. It was referred form this diagram that the maximum shear stress of the tunnel-ring joints under the Kocaeli earthquake was more considerable than that of other earthquakes.

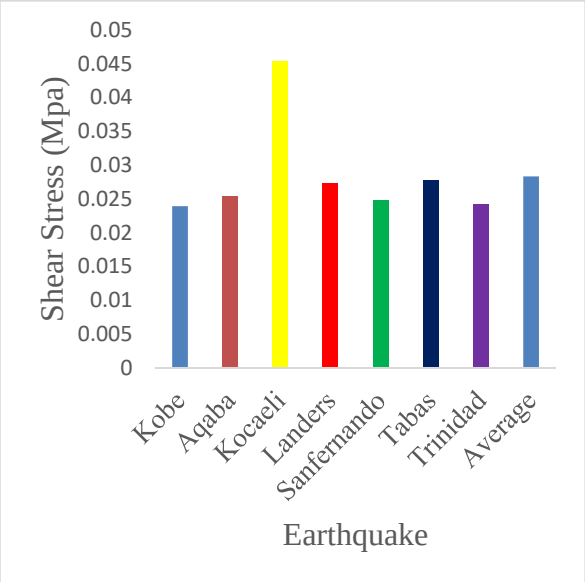


**Figure 12. Comparison of maximum shear stress for the critical joint under earthquakes**

***C) Investigating the Von-Mises Stress of Longitudinal Joints***

In the case of elements under normal and shear stress, Von-Mises stress was considered to be used in examining the stress. The Von-Mises stress relation for two-dimensional mode was as follows [31].

$$\sigma_V = \sqrt{\frac{1}{2}[(\sigma_{11})^2+(-\sigma_{11})^2] + 3(\sigma_{12}{}^2)} \quad (22)$$

In the above relation, $\sigma_{11}$ and $\sigma_{12}$ were normal stress and shear stress, respectively. Figure 13 displayed a comparison of Von-Mises stresses under 7 earthquake records for joint, which had a maximum Von-Mises stress under the influence of fibers. In 6 of the 7 given earthquakes to software, the maximum Von-Mises stress was observed at joint 3. With respect to the Japan Civil Engineering Association, stresses, after altering tunnel-ring from integrated to segmental, would be minimized at the formation position of longitudinal joints.

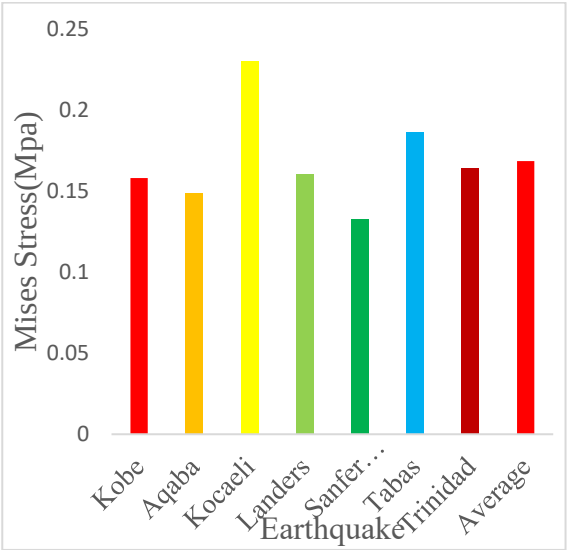


**Figure 13. Comparison of Von-Mises stresses under 7 earthquake records for the critical joint**

***D) Investigating Changes in the Normal Displacement of Longitudinal Joints***

Figure 14 illustrated comparison of the maximum normal displacement of tunnel critical joints under 7 earthquake records. This comparison was taken place at joint 4 in the case of 1.5% fibers under Kobe earthquake, at joint 6 in the 0% fibers under Aqaba earthquake and joint 3 in the 0% fibers under Landers earthquake, the joint 3 in 0.7% fibers under Trinidad earthquake, and joint 3 in 1.5% fibers under the other earthquakes. It was cleared in this diagram that the maximum normal displacement occurred under the Tabas earthquake.

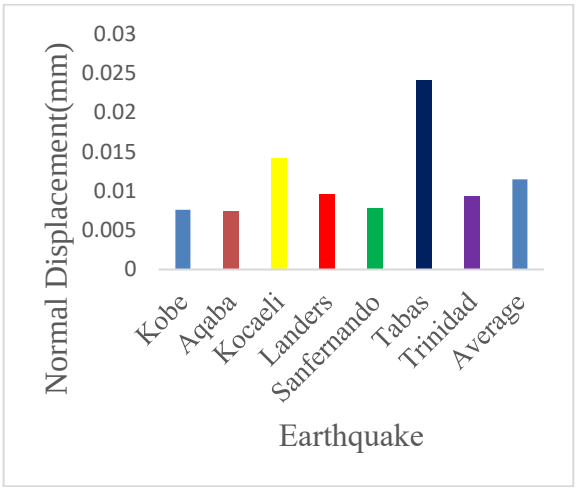


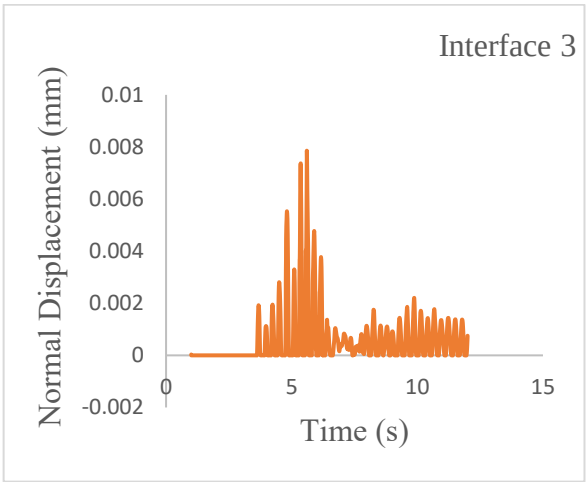


**Figure 14. Comparison of the maximum normal displacement of tunnel critical joints**

***E) Investigating Changes in Shear Displacement of Longitudinal Joints***

Figure 14 is related to a comparison of the maximum shear displacement of the tunnel critical joints under 7 earthquake records. This comparison was for joint 1 in the case of 0% fibers under the Kobe, Aqaba, and Landers earthquakes, and joint 1 in the 0.7 % fibers under the other earthquakes. This diagram showed that the maximum shear displacement was observed under the Kobe earthquake.

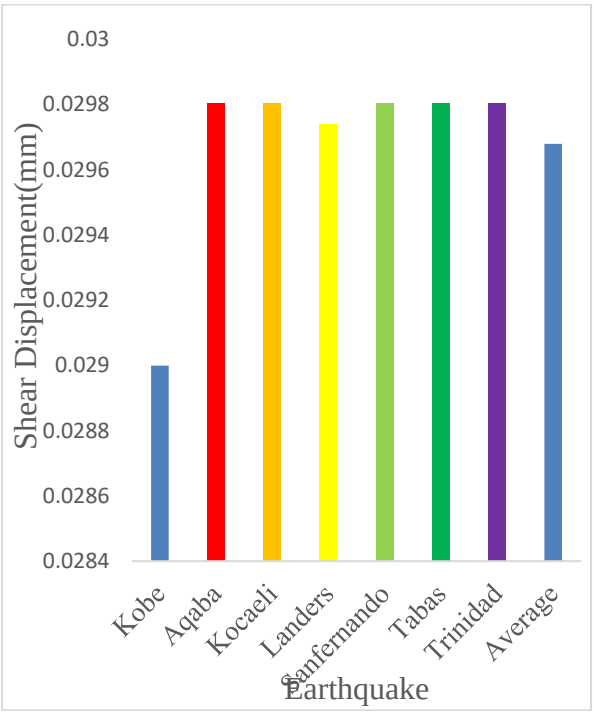


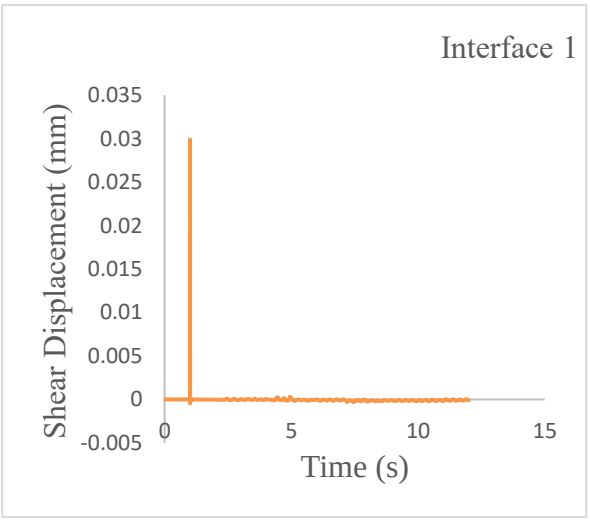


**Figure 15 revealed the maximum shear displacement history of joint 1 in the case of 0% fibers.**

## 9. Having an Eye on ACI 544.7R-16 Regulations

The ACI 544.7R-16 [32] regulation attempted to study various factors involved in the design and construction of tunnels by means of prefabricated concrete segments. One of these factors was the application of fiber-reinforced concrete. One part of this regulation dealt with the manner of drawing an moment-force diagram of the longitudinal joints of the tunnel under different

compressive and tensile strengths of fiber-reinforced concrete.

***A) Investigate the Moment-Force Diagram of Longitudinal Joints***

The following figure indicated the whole diagram of the moment-force for a longitudinal joint. In this figure, the diagram was portioned into three areas where each area was observed with its own relations. These three areas are presented by points A, B, and C.

The following part securitizes the analytical relations related to the moment and force of the points existed in the above figure and the equations related to the areas in the figure [28].

***Point A(Fig 4-1):***

$$P_0 = 0.85 f_c A_g = 0.85 f_c bh \quad (23)$$

$$P_n(max) = 0.8 P_0 \rightarrow P_n = 0.68 f_c bh \quad (24)$$

$$\varphi = 0.7 \rightarrow \varphi P_n = 0.476 f_c bh \quad (25)$$

$$\varphi M_n = 0 \quad (26)$$

The above relations were achieved for three fibers with the percentages of 0.7, 1, and 1.5 and compressive strengths used in the software and the characteristics of the water transmission tunnel of Amirkabir Dam.

*PFRC 0.7%:*

$$f_c = 41.1\ Mpa\ , b = 250mm\ , h = 1200mm \rightarrow \varphi P_n = 5869.08\ kN$$

*PFRC 1%:*

$$f_c = 43.11\ Mpa\ , b = 250mm\ , h = 1200mm \rightarrow \varphi P_n = 6156.108\ kN$$

*PFRC 1.5%:*

$$f_c = 44.77\ Mpa\ , b = 250mm\ , h = 1200mm \rightarrow \varphi P_n = 6393.156\ kN$$

***Point B(Fig 4-1):***

$$C_c = f_c \frac{bh}{2}\left(1 + \frac{c-h}{c}\right) \quad (27)$$

$$P_n = C_c \rightarrow 0.68 f_c bh = f_c \frac{bh}{2}\left(1 + \frac{c-h}{c}\right) \rightarrow c = 1.562h \quad (28)$$

$$P_n = C_c$$

$$f_{bot} = \frac{c-h}{c} f_c = \frac{0.562}{1.562} f_c = 0.36 f_c \quad (29)$$

$$y_c = \frac{h(2 \times 0.36 f_c + f_c)}{3(f_c + 0.36 f_c)} = \frac{1.72 h f_c}{4.08 f_c} \rightarrow y_c = 0.421h \quad (30)$$

$$C_c = \frac{(1 + 0.36) f_c}{2} bh = 0.68 f_c bh \quad (31)$$

$$M_n = C_c\left(\frac{h}{2} - y_c\right) = 0.68 f_c bh\left(\frac{h}{2} - 0.421h\right) = 0.68 f_c bh(0.78) \quad (32)$$

$$M_n = 0.053 f_c bh^2\ ;\ \varphi = 0.7 \rightarrow \varphi M_n = 0.037 f_c bh^2 \quad (33)$$

*PFRC 0.7%:*

$$f_c = 41.1\ Mpa\ , b = 250mm\ , h = 1200mm \rightarrow \varphi P_n = 5869.08\ kN$$

$$\varphi M_n = 547.452\ kN.m$$

*PFRC 1%:*

$$f_c = 43.11\ Mpa\ , b = 250mm\ , h = 1200mm \rightarrow \varphi P_n = 6156.108\ kN$$

$$\varphi M_n = 574.2252\ kN.m$$

*PFRC 1.5%:*

$$f_c = 44.77\ Mpa\ , b = 250mm\ , h = 1200mm \rightarrow \varphi P_n = 6393.156\ kN$$

$$\varphi M_n = 596.3364\ kN.m$$

***Point C(Fig 4-1):***

$$C_c = f_c \frac{bh}{2} \quad (34)$$

$$P_n = C_c \rightarrow P_n = f_c \frac{bh}{2}\ ;\ \varphi = 0.7 \rightarrow \quad (35)$$

$$\varphi P_n = 0.35 f_c bh \quad (36)$$

$$M_n = C_c\left(\frac{h}{2} - \frac{h}{3}\right) = C_c\left(\frac{h}{6}\right) = \frac{f_c}{12} bh^2 \rightarrow \quad (37)$$

$$\varphi M_n = 0.058 f_c bh^2 \quad (38)$$

*PFRC 0.7%:*

$f_c = 41.1\ Mpa\ , b = 250mm\ , h = 1200mm \rightarrow \varphi P_n = 4315.5\ kN$

$\varphi M_n = 858.168\ kN.m$

*PFRC 1%:*

$f_c = 43.11\ Mpa\ , b = 250mm\ , h = 1200mm \rightarrow \varphi P_n = 4526.55\ kN$

$\varphi M_n = 900.1368\ kN.m$

*PFRC 1.5%:*

$f_c = 44.77\ Mpa\ , b = 250mm\ , h = 1200mm \rightarrow \varphi P_n = 5641.02\ kN$

$\varphi M_n = 934.7976\ kN.m$

***Zone 2(Fig 4-1):***

$$P_n = C_c = f_c\left(1 + \frac{x}{x+h}\right)\frac{bh}{2}\ ;\ \varphi = 0.7 \quad (39)$$

$$y_c = \frac{h\left(\frac{2xf_c}{x+h}+f_c\right)}{3\left(f_c+\frac{x}{x+h}f_c\right)} = \frac{h\left(\frac{2x}{x+h}+1\right)}{3\left(1+\frac{x}{x+h}\right)} = \frac{h}{3}\frac{(3x+h)}{(2x+h)} \quad (40)$$

$$M_n = C_c\left(\frac{h}{2} - y_c\right) = f_c\left(\frac{2x+h}{x+h}\right)\frac{bh^2}{2}\left(\frac{1}{2} - \frac{3x+h}{3(2x+h)}\right)\ ;\ \varphi = 0.7 \quad (41)$$

***Zone 3:***

$$C_c = \frac{f_c(h-y)b}{2}\ ;\ C_t = \sigma_p yb \rightarrow P_n = C_c - C_t \quad (42)$$

$$P_n = \frac{f_c(h-y)b}{2} - \sigma_p yb\ ;\ \varphi_p = 0.34f^D \quad (43)$$

$$M_n = C_c\left(\frac{y}{3} + \frac{h}{6}\right) + C_t\left(\frac{h-y}{2}\right) \quad (44)$$

$$M_n = f_c\left(\frac{h-y}{2}\right)\left(\frac{y}{3} + \frac{h}{6}\right)b + \sigma_p yb\ (\frac{h-y}{2}) \quad (45)$$

$f^D$ in the above relation was representative of the concept of tensile stress.

The maximum normal stress in the longitudinal joints of the selected section of the Amirkabir tunnel was attributed to the joint 3 under the Kocaeli earthquake. Moment-force diagram was prepared for the percentages of 0.7, 1, and 1.5 of fibers for this joint through software output and the presented relations. Then, A, B, and C points were achieved. In order to fully draw the diagram, the point force should be gained, in which the moment point was equal to zero.

*PFRC 0.7%:*

$f_c = 41.1\ Mpa\ , b = 250mm\ , h = 1200mm\ ,$

$\sigma_p = 0.1866\ {}^{N}/_{mm^2}\ , M_n = 0$

$\rightarrow y = 1200 \rightarrow P_n = -55.98\ kN$

$f^D = 3.52\ {}^{N}/_{mm^2} \rightarrow \varphi_p = 1.196 \rightarrow \varphi P_n = -66.952$

*PFRC 1 %:*

$f_c = 43.11\ Mpa\ , b = 250mm\ , h = 1200mm\ ,$

$\sigma_p = 0.1943\ {}^{N}/_{mm^2}\ , M_n = 0$

$\rightarrow y = 1200 \rightarrow P_n = -58.290\ kN$

$f^D = 3.6\ {}^{N}/_{mm^2} \rightarrow \varphi_p = 1.224 \rightarrow \varphi P_n = -71.346$

*PFRC 1.5 %:*

$f_c = 44.77\ Mpa\ , b = 250mm\ , h = 1200mm\ ,$

$\sigma_p = 0.2165\ {}^{N}/_{mm^2}\ , M_n = 0$

$\rightarrow y = 1200 \rightarrow P_n = -64.950\ kN$

$f^D = 3.669\ {}^{N}/_{mm^2} \rightarrow \varphi_p = 1.247 \rightarrow \varphi P_n = -80.992$

Figure 16 indicated the anchor-force diagram of the joint 3 under the Kocaeli earthquake at different percentages of fibers. Given the figure, an increase in the fiber percentage made the diagram to be more open, and finally, the joint would be more resistant to more forces and moments. The joint in the points out of the diagram would be exposed to failure. The joint under the points inside the diagram was safe from failure, and the joint under the points on the diagram would be at risk of failure. The moment in the points placed on the vertical axis was 0, and the joint was put under a pure axial load.

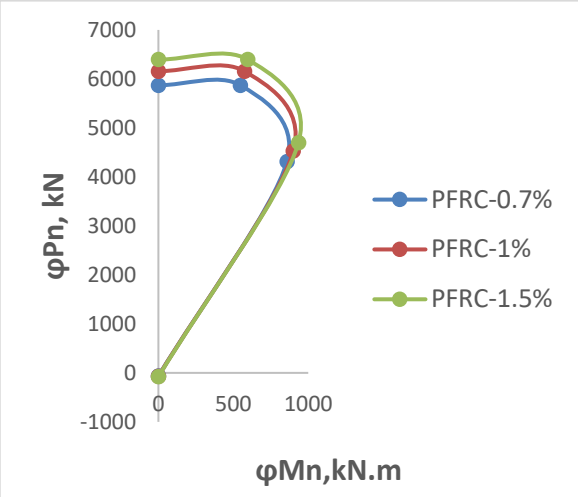


**Figure 16. Moment-force diagram of the joint 3 under the Kocaeli earthquake at different percentages of fibers**

## Conclusion

Rebars of grade 8 and 10 have been used to model the validation model, and according to the graphs of the article, the maximum displacement of the middle of the sample opening was 30 cm, and this displacement value has been applied in the model. The maximum force tolerated in the middle of the opening of the FE model for concrete without fibers was about 200 kN, which corresponds to the value of the diagram in the article. The maximum force tolerated in the middle of the opening of the software model for fiber concrete was about 220 kN. This value in the diagram of the article for fiber concrete was about 210 kN. As a result, the output obtained from the FE analysis was in good agreement with the output of the article for FRC.

Since the longitudinal joints were barely under shear, it is desirable that the fibers work more to reduce the normal displacements, which could be deduced from the results.

Due to the fact that in most of the examined parameters, the best possible state for the coating and longitudinal joints occurred for the state of 1.5 percentage of fibers, it could be concluded that the use of fibers with such volume percentage could be more suitable than other percentages of fibers.

By examining the relationships of ACI 544.7R-16 regulations and illustration of the moment-force diagram of joint No. 3 under the Kocaeli earthquake, it was concluded that the more the percentage of fibers increases, the wider the diagram could occur, as a result, the joint can withstand more force and moment.

## References

1. Mitelman, A. and D. Elmo, Analysis of tunnel support design to withstand spalling induced by blasting. Tunnelling and Underground Space Technology, 2016. 51: p. 354-361.
2. Nguyen, V.-Q., et al., Numerical simulation of damage evolution of Daikai station during the 1995 Kobe earthquake. Engineering Structures, 2020. 206: p. 110180.
3. Mayoral, J.M., S. Argyroudis, and E. Castañon, Vulnerability of floating tunnel shafts for increasing earthquake loading. Soil Dynamics and Earthquake Engineering, 2016. 80: p. 1-10.
4. Hashash, Y.M., et al., Seismic design and analysis of underground structures. Tunnelling and underground space technology, 2001. 16(4): p. 247-293.
5. Severcan, M.H., Prediction of splitting tensile strength from the compressive strength of concrete using GEP. Neural Computing and Applications, 2012. 21: p. 1937-1945.
6. Garas, G., H. El Kady, and A. El Alfy, Developing a new combined structural roofing system of domes and vaults supported by cementitious straw bricks. ARPN Journal of Engineering and Applied Sciences, under publication, 2010.
7. Tafraoui, A., G. Escadeillas, and T. Vidal, Durability of the ultra high performances concrete containing metakaolin. Construction and Building Materials, 2016. 112: p. 980-987.
8. Mobasher, B., M&S highlight: Naaman & Reinhardt (2006), Proposed classification of HPFRC composites based on their tensile response. Materials and Structures, 2022. 55(2): p. 49.
9. Lee, M. and B. Barr, An overview of the fatigue behaviour of plain and fibre reinforced concrete. Cement and Concrete Composites, 2004. 26(4): p. 299-305.

10. Paul, S.C., G.P. van Zijl, and B. Šavija, Effect of fibers on durability of concrete: A practical review. Materials, 2020. 13(20): p. 4562.
11. Bongarde, U. and V. Shinde, Review on natural fiber reinforcement polymer composites. International Journal of Engineering Science and Innovative Technology, 2014. 3(2): p. 431-436.
12. Wang, K. and H. Le, The Development of Cement-Based, Intumescent and Geopolymer Fire-Retardation Coatings for Metal Structures: A Review. Coatings, 2023. 13(3): p. 495.
13. Singleton, A., et al., On the mechanical properties, deformation and fracture of a natural fibre/recycled polymer composite. Composites Part B: Engineering, 2003. 34(6): p. 519-526.
14. Shibata, S., Y. Cao, and I. Fukumoto, Press forming of short natural fiber-reinforced biodegradable resin: Effects of fiber volume and length on flexural properties. Polymer testing, 2005. 24(8): p. 1005-1011.
15. Wang, Y., et al., Quantitative evaluation of the characteristics of air voids and their relationship with the permeability and salt freeze–thaw resistance of hybrid steel-polypropylene fiber–reinforced concrete composites. Cement and Concrete Composites, 2022. 125: p. 104292.
16. Habel, K., E. Denarié, and E. Brühwiler, Experimental investigation of composite ultra-high-performance fiber-reinforced concrete and conventional concrete members. ACI Structural Journal, 2007. 104(1): p. 93.
17. Qiu, M., et al., Effect of reinforcement ratio, fiber orientation, and fiber chemical treatment on the direct tension behavior of rebar-reinforced UHPC. Construction and Building Materials, 2020. 256: p. 119311.
18. Ferrara, L., Y.-D. Park, and S.P. Shah, A method for mix-design of fiber-reinforced self-compacting concrete. Cement and concrete research, 2007. 37(6): p. 957-971.
19. JP, A.D.K. and N. Sakthieswaran, Strength and stability characteristics of GGBS and red mud based geopolymer concrete incorporated with hybrid fibres. Indian Concrete Journal, 2015: p. 66.
20. Fall, D., et al., Two-way slabs: Experimental investigation of load redistributions in steel fibre reinforced concrete. Engineering Structures, 2014. 80: p. 61-74.
21. Ramoni, M. and G. Anagnostou, Tunnel boring machines under squeezing conditions. Tunnelling and Underground Space Technology, 2010. 25(2): p. 139-157.
22. Namy, M., J.-P. Charron, and B. Massicotte, Structural behavior of cast-in-place and precast concrete barriers subjected to transverse static loading and anchored to bridge deck overhangs. Canadian Journal of Civil Engineering, 2015. 42(2): p. 120-129.
23. Zheng, G., et al., Numerical study of the Soil-Tunnel and Tunnel-Tunnel interactions of EPBM overlapping tunnels constructed in soft ground. Tunnelling and Underground Space Technology, 2022. 124: p. 104490.
24. Conforti, A., et al., Precast tunnel segments reinforced by macro-synthetic fibers. Tunnelling and Underground Space Technology, 2017. 63: p. 1-11.
25. Standard, B., Eurocode 2: Design of concrete structures—. Part, 2004. 1(1): p. 230.
26. Hsu, L. and C.-T. Hsu, Complete stress—strain behaviour of high-strength concrete under compression. Magazine of concrete research, 1994. 46(169): p. 301-312.
27. Taerwe, L. and S. Matthys, Fib model code for concrete structures 2010. 2013, Ernst & Sohn, Wiley.
28. Choi, Y. and R.L. Yuan, Experimental relationship between splitting tensile strength and compressive strength of GFRC and PFRC. Cement and Concrete Research, 2005. 35(8): p. 1587-1591.
29. Chi, Y., et al., Finite element modeling of steel-polypropylene hybrid fiber reinforced concrete using modified concrete damaged plasticity. Engineering Structures, 2017. 148: p. 23-35.
30. Pariseau, W.G., Design analysis in rock mechanics. 2017: CRC Press.
31. Segalman, D.J., et al., An efficient method for calculating RMS von Mises stress in a random vibration environment. Journal of Sound and Vibration, 2000. 230(2): p. 393-410.
32. Institute, A.C., ACI Manual of Concrete Practice, 2017. 2017: ACI, American Concrete Institute.